tylphosphine (θ = 132°) clearly, by visual inspection and EPR signals, gave the product **c**, but crystals were not obtained due to high solubility of the products, even in hexane. The species **b** can therefore only be intercepted if the phosphine is not too sterically demanding or too oleophilic. Similar constraints will limit success in obtaining crystalline products from bulky silanes.

The coordinatively unsaturated species **b** is apparently very reactive, as are the alkyltitanocene(III) analogues,[21] and any factor that leads to an increase in its concentration is also likely to lead to decomposition. The facile dissociation of the phosphine ligand at room temperature on dissolution of the pure complexes is the most likely cause of their rapid decomposition. The question of how Ti(III) is formed in these reactions remains an open one. Two routes seem equally plausible at the present time. The first is a homolytical bond cleavage of an unstable Ti(IV) intermediate. The bond involved could conceivably be a Ti–H, a Ti–C, or a Ti–Si bond. A second route would be the conproportionation of titanocene, resulting from a two-electron reduction process such as reductive elimination or two one-electron reduction steps, with a Ti(IV) species. We are continuing to seek further evidence to discriminate between these two possibilities.

Conclusion

The silyltitanocene(III) compounds described above are, to our knowledge, the only examples of structurally characterized mononometallic compounds with a Ti(III)–group 14 bond. Together with the bimetallic species **1** and **2**, they show that there is a rich chemistry of relatively stable silyl species associated with this metal in its oxidation state (III). This situation contrasts with the corresponding carbon chemistry, where alkyl compounds of titanocene(III) are thermally unstable, and no compounds, with or without donor ligands, have been isolated and structurally characterized. Successful isolation of these novel silylphosphine compounds seems to depend largely on the importance of steric interactions of the substituent groups on the silicon and on phosphorus in the molecule. Their reactivity, particularly with respect to understanding the mechanism of titanocene-catalyzed dehydrogenative coupling of silanes, is the subject of further study.

Acknowledgment. Financial support from the Natural Science and Engineering Research Council of Canada and the Fonds FCAR de Quebec is gratefully acknowledged by J.F.H. We are grateful to J. Hénique for technical assistance.

Supplementary Material Available: Tables of fractional atomic coordinates, isotropic and anistropic thermal parameters, bond lengths, bond angles, and least-squares planes for **5** and **7** (16 pages); observed and calculated structure factors for **5** and **7** (20 pages). Ordering information is given on any current masthead page.

Preparative, Structural, and Magnetic Studies of 2-Hydroxypyridinate Complexes of Diruthenium(II)

F. Albert Cotton,*[1a] Tong Ren,[1a] and Judith L. Eglin[1b]

Contribution from the Department of Chemistry and Laboratory of Molecular Structure and Bonding, Texas A&M University, College Station, Texas 77843, and Department of Chemistry, Michigan State University, East Lansing, Michigan 48824. *Received September 5, 1989*

Abstract: Three new compounds each containing the Ru_2^{4+} core bridged by four 6-X-2-hydroxypyridinate anions (mhp^-, X = CH_3; chp^-, X = Cl; bhp, X = Br) have been prepared in good yields (60–90%) from $Ru_2(O_2CCH_3)_4$, and each one has been characterized by X-ray crystallography and magnetic susceptibility measurements from ca. 5 to ca. 300 K. (**1**) Red-brown $Ru_2(mhp)_4$ crystallizes in space group *Pbca* with a = 16.165 (3) Å, b = 18.638 (5) Å, c = 15.745 (3) Å, V = 4744 (3) Å^3, and Z = 8; (**2**) brown $[Ru_2(chp)_4]_2 \cdot CH_2Cl_2$ crystallizes in space group $P\bar{1}$ with a = 14.489 (7) Å, b = 15.514 (10) Å, c = 11.703 (2) Å, α = 101.13 (3)°, β = 103.60 (3)°, γ = 100.03 (4)°, V = 2452 (4) Å^3, and Z = 2; (**3**) dark-red $Ru_2(bhp)_4$ crystallizes in space group $P2_1/c$ with a = 14.996 (5) Å, b = 13.464 (6) Å, c = 16.130 (5) Å, β = 109.22 (3)°, V = 3075 (4) Å^3, and Z = 4. The structure of $Ru_2(mhp)_4$ has Ru–Ru = 2.235 (1) Å and a torsion angle of 6.2°, with a symmetrical ligand arrangement placing like atoms (i.e., N's or O's) trans at each end. The $Ru_2(bhp)_4$ molecule is very similar, with Ru–Ru = 2.259 (1) Å and a torsion angle of 1.17°. The chp compound has tetranuclear molecules consisting of two approximately (but not rigorously) identical halves bonded by axial O–Ru bonds. Within each half, three chp ligands are oriented in the same direction. Both Ru–Ru distances are 2.247 (1) Å, and the twist angles are 19.9° and 20.8°, respectively. All three compounds show essentially the same magnetic behavior, indicating that they have a spin-triplet/orbital-singlet ground state derived from a $\delta^{*2}\pi^{*2}$ electron configuration. Zero-field splitting of the state to give a lower singlet (M_S = 0) causes the magnetic moment to aproach zero as $T \rightarrow 0$ K.

Although $M_2(xhp)_4$ compounds of other elements were known earlier,[2] the first $Ru_2(xhp)_4$ compound was reported in 1980, namely $Ru_2(mhp)_4$.[3] In fact, this was the first quadruply bridged Ru_2^{4+} complex of any type to be isolated and characterized. While it had been clear since 1975, from the electrochemical study[4] of $Ru_2(O_2CC_3H_7)_4Cl$, that $Ru_2(O_2CR)_4L_2$ compounds should be obtainable, the first one was actually reported only in 1984.[5] Following this, a number of others have been described.[6-9]

(1) (a) Texas A&M University. (b) Michigan State University.

(2) (a) Cotton, F. A.; Walton, R. A. *Multiple Bonds Between Metal Atoms*; John Wiley & Sons: New York, 1982. (b) Abbreviations: xhp^- represents a substituted 2-hydroxypyridinate anion with X in the 6-position. mhp^-, chp^-, and bhp^- are the 6-methyl, 6-chloro, and 6-bromo species, respectively.

(3) (a) Berry, M.; Garner, C. D.; Hillier, I. H.; MacDowell, A. A.; Clegg, W. *Inorg. Chim. Acta* **1981**, *53*, L61. (b) Clegg, W. *Acta Crystallogr., Sect. B: Struct. Crystallogr. Cryst. Chem.* **1980**, *B36*, 3112.

(4) Cotton, F. A.; Pederson, E. *Inorg. Chem.* **1975**, *14*, 388.

(5) Lindsay, A. J.; Tooze, R. P.; Motevalli, M.; Hursthouse, M. B.; Wilkinson, G. *J. Chem. Soc., Chem. Commun.* **1984**, 1383.

(6) Lindsay, A. J.; Wilkinson, G.; Motevalli, M.; Hursthouse, M. B. *J. Chem. Soc. Dalton Trans.* **1987**, *2723*.

(7) Spohn, M.; Strahle, J.; Hiller, W. *Z. Naturforsch., B: Anorg. Chem., Org. Chem.* **1986**, *41*, 541.

(8) Cotton, F. A.; Miskowski, V. M.; Zhong, B. *J. Am. Chem. Soc.* **1989**, *111*, 6177.

0002-7863/90/1512-3439$02.50/0

Altogether, six $Ru_2(O_2CR)_4L_2$ compounds have been characterized structurally, and the Ru–Ru distances are all in the range 2.260 (3)–2.276 (3) Å. In all cases, magnetic susceptibility measurements at room temperature indicate the presence of two unpaired electrons.

There has been considerable discussion about the electron configuration giving rise to the ground state in these $Ru_2(O_2CR)_4L_2$ molecules. The possibilities consistent with two unpaired electrons are $\sigma^2\pi^4\delta^2\pi^{*3}\delta^*$ and $\sigma^2\pi^4\delta^2\pi^{*2}\delta^{*2}$, which may be written in abbreviated form as $\pi^{*3}\delta^*$ and $\pi^{*2}\delta^{*2}$. The SCF–Xα calculations of Norman et al.[10] suggested the former, and presumably for this reason, most authors[6,7,11] favored this, though some remained undecided.[12] There was one unequivocal vote[13] for the $\pi^{*2}\delta^{*2}$ configuration, based on bond length considerations. The reasoning was that from the bond length of ca. 2.27 Å found in $Ru_2(O_2CR)_4^+$ species, which have $\pi^{*2}\delta^*$ configurations, addition of a π^* electron should cause appreciable lengthening of the Ru–Ru bond (by ca. 0.07 Å) whereas, in fact, no such lengthening occurs. this is consistent with adding a δ^* electron, which should have little effect on the Ru–Ru distance, thereby arriving at a $\pi^{*2}\delta^{*2}$ configuration.

In 1989, studies of the temperature dependence of the magnetic susceptibilities of several $Ru_2(O_2CR)_4L_2$ compounds[8,9] afforded conclusive evidence for the $\delta^{*2}\pi^{*2}$ configuration. In writing the orbitals in this order, we do not imply that the orbital energies are necessarily in the order $\delta^* < \pi^*$, since the role of interelectronic energies in determining the ground state may be important. Indeed, a suggested interpretation of the photoelectron spectrum[14] of $Ru_2(O_2CCF_3)_4$ assigned the three lowest energy peaks (at 8.49, 9.00, and 9.66 eV) to loss of δ^*, π^*, and δ electrons, respectively.

In the meantime, several studies of triazeno complexes, $Ru_2(RNNNR)_4$, provided evidence that with these very basic ligands the δ^* orbitals are pushed well above the π^* orbitals.[15,16] This should cause a π^{*4} configuration to prevail with a Ru–Ru bond distance much greater than those in the carboxylates (ca. 2.26 Å). Experimentally, this is exactly what is observed,[13] $Ru_2(tolNNNtol)_4$ being diamagnetic with an Ru–Ru distance of 2.417 (2) Å.

The results just summarized led us to formulate the question to which the work reported here was addressed. Given that for the least basic ligands, RCO_2^-, the δ^* orbital is low enough in energy for the $\delta^{*2}\pi^{*2}$ to prevail, while for the most basic ligands, $R_2N_3^-$, the δ^* orbital is so high in energy that a π^{*4} configuration prevails, what will happen with ligands of intermediate basicity? Ligands of intermediate basicity would be those with one oxygen atom and one nitrogen atom as the coordinating atoms, and the usual examples are amido anions, $RC(O)NR'^-$, and 2-hydroxypyridine anions.

We chose to deal with the latter type because one such compound had already been reported,[3a] namely $Ru_2(mhp)_4$, as mentioned at the outset. Moreover, the results that had been presented for this compound seemed to us to favor the $\delta^{*2}\pi^{*2}$ configuration, although the previous authors[3a] had proposed the $\pi^{*3}\delta^*$ alternative. The basis for their choice seemed flawed. The PE spectrum is not inconsistent with a $\pi^{*2}\delta^{*2}$ configuration, and the Ru–Ru bond length of 2.238 (1) Å is clearly in favor of that configuration. In view of the previous use of magnetic data to support the $\pi^{*2}\delta^{*2}$ configuration in $Ru_2(O_2CR)_4L_2$ compounds, it seemed likely that a similar approach would be appropriate here.

The previous preparation of $Ru_2(mhp)_4$ had been carried out before $Ru_2(O_2CR)_4$ compounds were available as starting materials, and the method used was clearly no longer appropriate. The $Ru_2(xhp)_4$ compounds have now been obtained efficiently from $Ru_2(O_2CCH_3)_4$.

Experimental Section

All reactions were performed under argon in standard Schlenkware. $Ru_2(OAc)_4$ was prepared according to the established procedure.[6] 2-Hydroxy-6-methylpyridine (Hmhp), 6-chloro-2-pyridinol (Hchp), and sodium methoxide were purchased from Aldrich Chemical Co. 6-Bromo-2-pyridinol (Hbhp) was synthesized by the hydrolysis of 2,6-dibromopyridine in a *t*-BuOK/*t*-BuOH mixture according to a literature method.[17] All solvents used were of reagent grade or better from commercial sources and freshly distilled under N_2 with suitable drying reagents.

Reaction of $Ru_2(OAc)_4$ with Hmhp. (A) Hmhp was sublimed before use. In a typical reaction, 0.216 of NaOMe (4 mmol) and 0.44 g of Hmhp (4 mmol) were stirred in 25 mL of MeOH until all Hmhp dissolved. Then 0.44 g of $Ru_2(OAc)_4$ (1 mmol) was added to this solution. This yellow-brown suspension was stirred 3 h at room temperature, after which the solution became clear with some microcrystalline material deposited on the wall. The reaction mixture was evaporated to dryness under vacuum, and the solid residue was treated with 20 mL of benzene. The yellow-brown extract was filtered through a fine glass frit, then evaporated, and dried under vacuum to give a fine yellow powder, yield ca. 0.57 g (89%). The compound is very air sensitive in solution, which turned to purple immediately on the exposure to air. But the solid can be handled in the air for several minutes without observable degradation. The brown-red crystals (**1**) were grown by layering a benzene solution of the compound with hexane. (B) By a procedure very similar to procedure A given below for $[Ru_2(chp)_4]_2$, the yellow-brown product was separated in about 70% yield. The single crystals (**1'**) were grown from the layering of the dichloromethane solution with Et_2O.

Reaction of $Ru_2(OAc)_4$ with Hchp. (A) In a typical reaction, 0.22 g of $Ru_2(OAc)_4$ (0.5 mmol) and 0.39 g of Hchp (3 mmol) were well mixed, and the resultant mixture was then heated at 130 °C under argon for about 30 min. The yellow-brown mixture gradually became darker during the course of heating, while acetic acid was evolved and condensed on the wall of the flask. Acetic acid and excess Hchp were pumped off under vacuum. The dark solid residue was extracted with 15 mL of benzene. The yellow-brown extract was evaporated and dried under vacuum to give a yellow-green powder, yield ca. 0.24 g (67%). This compound, like the previous one, is also very air sensitive in solution. The dark crystals (**2**) suitable for X-ray study were obtained from the layering of the dichloromethane solution with ether. (B) By a procedure similar to that used for **1**, a yellow-green product was isolated in 60% yield. This was then obtained as single crystals (**2'**) from CH_2Cl_2 solution by layering with Et_2O.

Reaction of $Ru_2(OAc)_4$ with Hbhp. A procedure similar to Hchp reaction A was applied. The dark residue from the reaction was treated with benzene to give a dark brown solution, which was then dried under vacuum to give a yellow-brown powder. Yields were usually around 70%. Dark red crystals (**3**) were grown by the layering of a benzene solution with hexane.

X-ray Crystallography. For **1**, a blocklike crystal was mounted under mineral oil in a capillary tube. Indexing revealed an orthorhombic cell, and Laue class *mmm* was confirmed by an oscillation photograph. From the systematic absences the space group was uniquely assigned as *Pbca* (No. 61). Examination of the **1'** crystal on the diffractometer showed it to be the same as **1**. For **2** a wedgelike crystal was mounted on a quartz fiber with epoxy glue. Indexing gave a triclinic cell. For **2'** an initial indexing gave the same unit cell as **2** and revealed that **2** and **2'** are actually the same compound. For **3** a platelike crystal was mounted on a quartz fiber with epoxy glue. Indexing gave a monoclinic cell, and Laue symmetry was confirmed by oscillation photograph. The space group was determined as $P2_1/c$ (No. 14) based on the systematic absences. The main crystallographic parameters are summarized in Table I, while other procedural details are provided in supplementary material.

All of these structures are solved and refined by the following routine. The metal atoms and the atoms coordinated to them were located by the Patterson method as programmed in SHELX-86. The other non-hydrogen atoms were then introduced by an alternating series of difference Fourier maps and least-squares refinements in the SDP package. All of the non-hydrogen atoms were refined anisotropically to low residuals. Most of the hydrogen atoms were then found by difference Fourier maps, and the coordinates of the rest were calculated. For **1** the hydrogen atoms

(9) Maldivi, P.; Giroud-Godquin, A.; Marchon, J.; Guillon, D.; Skoulios, A. *Chem. Phys. Lett.* **1989**, *157*, 552.
(10) Norman, J. G.; Renzoni, G. E.; Case, D. A. *J. Am. Chem. Soc.* **1979**, *101*, 5256.
(11) Noels, A. F.; Demonceau, A.; Carlier, E.; Hubert, A. J.; Marquez-Silva, R.; Sanchez-Delgado, R. A. *J. Chem. Soc., Chem. Commun.* **1988**, 783.
(12) Clark, D. L.; Green, J. C.; Redfern, C. M. *J. Chem. Soc. Dalton Trans.* **1989**, 1037.
(13) Cotton, F. A.; Matusz, M. *J. Am. Chem. Soc.* **1988**, *110*, 5761.
(14) Clark, D. L.; Green, J. C.; Redfern, C. M.; Quelch, G. E.; Hillier, I. H.; Guest, M. F. *Chem. Phys. Lett.* **1989**, *154*, 326.
(15) Rizzi, G. A.; Casarin, M.; Tondello, E.; Piraino, P.; Granozzi, G. *Inorg. Chem.* **1987**, *26*, 3406.
(16) Cotton, F. A.; Feng, X. *Inorg. Chem.* **1989**, *28*, 1180.
(17) Newkomb, G. R.; Brousard, S. K.; Sauer, J. D. *Synthesis* **1974**, 706.

Table I. Crystallographic Data for 1-3

formula	$Ru_2O_4C_{24}H_{24}$ (1)	$Ru_4Cl_{10}O_8N_8C_{41}H_{26}$ (2)	$Ru_2Br_4O_4N_4C_{29}H_{21}$ (3)
formula weight	634.62	1517.52	1011.29
space group	*Pbca* (No. 61)	$P\bar{1}$ (No. 2)	$P2_1/c$ (No. 14)
a, Å	16.165 (3)	14.489 (7)	14.996 (5)
b, Å	18.638 (5)	15.514 (10)	13.464 (6)
c, Å	15.745 (3)	11.703 (2)	16.130 (5)
α, deg		100.13 (3)	
β, deg		103.60 (3)	109.22 (3)
γ, deg		100.03 (4)	
V, Å^3	4744 (3)	2452 (4)	3075 (4)
Z	8	2	4
d_{calc}, g/cm^3	1.777	2.055	2.184
μ(Mo Kα), cm^{-1}	12.9	18.0	61.6
radiation monochromated in incident beam λ(Mo Kα), Å	0.71073	0.71073	0.71073
temp, °C	20	−80	−80
transmissn factors: max, min	1.00, 0.91	1.00, 0.72	1.00, 0.68
R^a	0.031	0.037	0.050
$R_w{}^b$	0.045	0.053	0.067

$^a R = \sum||F_o| - |F_c||/\sum|F_o|$. $^b R_w = [\sum w(|F_o| - |F_c|)^2/\sum w|F_o|^2]^{1/2}$; $w = 1/\sigma^2(|F_o|)$. ^{c}Quality-of-fit $= [\sum w(|F_o| - |F_c|)^2/(N_{obsd} - N_{param})]^{1/2}$

were refined isotropically. For **2** and **3** the hydrogen atoms were included only in the final calculations of the scale factors. From X-ray structure determination, **1-3** were found out to be $Ru_2(mhp)_4$, $[Ru_2(chp)_4]_2 \cdot CH_2Cl_2$, and $Ru_2(bhp)_4 \cdot 1.5C_6H_6$, respectively.

Physical Measurements. The magnetic susceptibility measurement were carried out on the SQUID (superconducting quantum interference device) at Michigan State University. The samples were all quenched in a field of 5 kG.

Results

Preparations. In the earlier synthesis of $Ru_2(mhp)_4$,[3a] $Ru_2(OAc)_4Cl$ was reacted with NaOMe to give the product in only 8% yield. Conversion of the starting (II, III) compound to the desired (II, II) compound depended on an uncontrolled reduction or disproportionation. In our synthesis of the tetra(2-hydroxypyridinato)diruthenium(II) compounds, $Ru_2(OAc)_4$ was used instead, which guaranteed a clean, high-yield reaction. For **1** the reaction equation for method A is presumably as follows

$$Ru_2(OAc)_4 + 4Na(mhp) \rightarrow Ru_2(mhp)_4 + 4NaOAc$$

which is comparable to the reactions used for the synthesis of the analogous Cr and Mo compounds. A preparation employing molten Hmhp gave the same product. The $[Ru_2(chp)_4]_2$ compound was initially synthesized by a molten reaction (method A), according to the following equation

$$Ru_2(OAc)_4 + 4Hchp \rightarrow [Ru_2(chp)_4]_2 + 4HOAc$$

After the molecular structure was found to be quite different from that of the $Ru_2(mhp)_4$ and $Ru_2(bhp)_4$ compounds (see below), a low-temperature reaction (method B) was carried out. The structure of the product, however, turned out to be same as the previous one, which indicates that this unusual structure is not a result of the reaction conditions. Due to the extreme air sensitivity, the $Ru_2(mhp)_4$ sample for the magnetic susceptibility measurement was treated with Na/Hg before the recrystallization to minimize the content of the oxidized form.

Molecular Structures. $Ru_2(mhp)_4$. The structure of this compound was reported before,[3b] but as a CH_2Cl_2 solvate, and the space group was $P2_1/c$. In our case the compound crystallized from benzene without any solvation in the orthorhombic space group *Pbca*. The molecular structure is essentially the same as the previous one. The metal-metal distance of 2.235 (1) Å (which is 0.003 Å shorter than the previously reported one) is the shortest Ru-Ru distance ever recorded. The average torsional angle of 6.2° is almost twice that in the CH_2Cl_2 solvate. The ORTEP drawing (Figure 1) shows that the molecule possesses an approximate D_{2d} geometry. The important bond lengths and bond angles are listed in Table II, while the torsional angles (N-M-M-O) are listed in Table V.

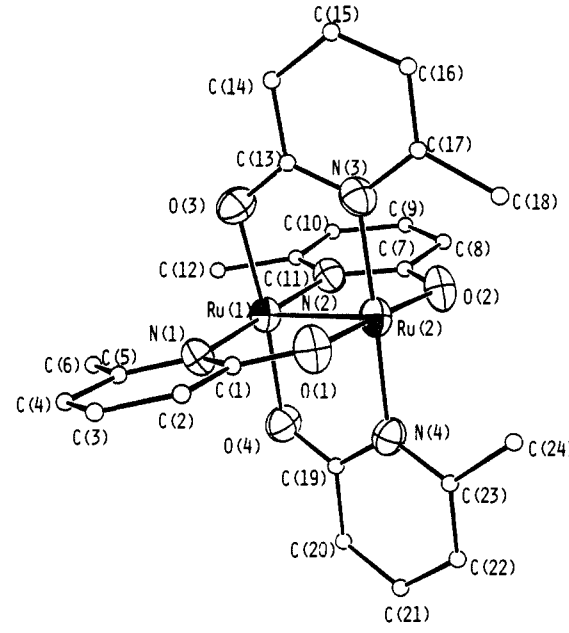

Figure 1. ORTEP drawing of $Ru_2(mhp)_4$.

Table II. Selected Bond Distances (Å) and Angles (deg) for $Ru_2(mhp)_4$

Bond Distances

atom 1-atom 2	distance[a]	atom 1-atom 2	distance[a]
Ru(1)-Ru(2)	2.235 (1)	O(1)-C(1)	1.297 (6)
Ru(1)-O(3)	2.051 (3)	O(2)-C(7)	1.296 (6)
Ru(1)-O(4)	2.044 (3)	O(3)-C(13)	1.289 (7)
Ru(1)-N(1)	2.076 (4)	O(4)-C(19)	1.289 (6)
Ru(1)-N(2)	2.084 (4)	N(1)-C(1)	1.361 (6)
Ru(2)-O(1)	2.054 (3)	N(2)-C(7)	1.368 (6)
Ru(2)-O(2)	2.046 (3)	N(3)-C(13)	1.360 (7)
Ru(2)-N(3)	2.095 (4)	N(4)-C(19)	1.370 (7)
Ru(2)-N(4)	2.087 (4)		

Bond Angles

atom 1-atom 2-atom 3	angle[a]	atom 1-atom 2-atom 3	angle[a]
Ru(2)-Ru(1)-O(3)	92.5 (1)	O(1)-Ru(2)-N(4)	89.5 (1)
Ru(2)-Ru(1)-O(4)	92.17 (9)	O(2)-Ru(2)-N(3)	89.4 (2)
Ru(2)-Ru(1)-N(1)	89.6 (1)	O(2)-Ru(2)-N(4)	90.8 (2)
Ru(2)-Ru(1)-N(2)	88.9 (1)	N(3)-Ru(2)-N(4)	178.0 (2)
O(3)-Ru(1)-O(4)	174.9 (1)	Ru(2)-O(1)-C(1)	119.8 (3)
O(3)-Ru(1)-N(1)	88.2 (1)	Ru(2)-O(2)-C(7)	118.9 (3)
O(3)-Ru(1)-N(2)	90.9 (1)	Ru(1)-O(3)-C(13)	118.9 (3)
O(4)-Ru(1)-N(1)	89.8 (2)	Ru(1)-O(4)-C(19)	119.7 (3)
O(4)-Ru(1)-N(2)	91.2 (2)	Ru(1)-N(1)-C(1)	119.1 (3)
N(1)-Ru(1)-N(2)	178.2 (1)	Ru(1)-N(2)-C(7)	119.2 (3)
Ru(1)-Ru(2)-O(1)	91.72 (9)	Ru(2)-N(3)-C(13)	118.8 (3)
Ru(1)-Ru(2)-O(2)	92.67 (9)	Ru(2)-N(4)-C(19)	118.6 (3)
Ru(1)-Ru(2)-N(3)	88.7 (1)	O(1)-C(1)-N(1)	119.2 (4)
Ru(1)-Ru(2)-N(3)	89.3 (1)	O(2)-C(7)-N(2)	119.4 (4)
O(1)-Ru(2)-O(2)	175.6 (1)	O(3)-C(13)-N(3)	120.0 (5)
O(1)-Ru(2)-N(3)	90.4 (1)	O(4)-C(19)-N(4)	119.4 (5)

[a] Numbers in parentheses are estimated standard deviations in the least significant digits.

$Ru_2(bhp)_4$. The selected bond lengths and angles and selected torsional angles are listed in Tables III and V, respectively. An ORTEP drawing, presented in Figure 2, shows that the coordination mode of the ligand is same as that in $Ru_2(mhp)_4$. The Ru-O and Ru-N distances are in the same range of those in $Ru_2(mhp)_4$ and $[Ru_2(chp)_4]_2$, but $Ru_2(bhp)_4$ has the longest Ru-Ru distance (2.259 (1) Å) and smallest N-M-M-O torsional angles among the three compounds.

$[Ru_2(chp)_4]_2$. The selected bond lengths and bond angles and selected torsional angles are given in Tables IV and V, respectively.

Table III. Selected Bond Distances (Å) and Angles (deg) for $Ru_2(bhp)_4 \cdot 1.5C_6H_6$

Bond Distances

atom 1–atom 2	distance[a]	atom 1–atom 2	distance[a]
Ru(1)–Ru(2)	2.259 (1)	O(1)–C(1)	1.297 (11)
Ru(1)–O(1)	2.041 (6)	O(2)–C(6)	1.296 (11)
Ru(1)–O(2)	2.038 (6)	O(3)–C(11)	1.290 (13)
Ru(1)–N(3)	2.091 (7)	O(4)–C(16)	1.282 (9)
Ru(1)–N(4)	2.103 (7)	N(1)–C(1)	1.380 (12)
Ru(2)–O(3)	2.039 (6)	N(2)–C(6)	1.362 (12)
Ru(2)–O(4)	2.036 (6)	N(3)–C(11)	1.374 (10)
Ru(2)–N(1)	2.098 (7)	N(4)–C(16)	1.372 (13)
Ru(2)–N(2)	2.063 (8)		

Bond Angles

atom 1–atom 2–atom 3	angle[a]	atom 1–atom 2–atom 3	angle[a]
Ru(2)–Ru(1)–O(1)	92.2 (2)	O(3)–Ru(2)–N(2)	90.4 (3)
Ru(2)–Ru(1)–O(2)	92.7 (2)	O(4)–Ru(2)–N1)	92.0 (3)
Ru(2)–Ru(1)–N(3)	88.8 (2)	O(4)–Ru(2)–N(2)	89.5 (3)
Ru(2)–Ru(1)–N(4)	88.7 (2)	N(1)–Ru(2)–N2)	176.9 (3)
O(1)–Ru(1)–O(2)	175.0 (3)	Ru(1)–O(1)–C(1)	121.1 (6)
O(1)–Ru(1)–N(3)	91.1 (3)	Ru(1)–O(2)–C(6)	119.0 (6)
O(1)–Ru(1)–N(4)	89.2 (3)	Ru(2)–O(3)–C(11)	119.8 (5)
O(2)–Ru(1)–N(3)	88.6 (3)	Ru(2)–O(4)–C(16)	121.5 (6)
O(2)–Ru(1)–N(4)	91.4 (3)	Ru(2)–N(1)–C(1)	119.4 (6)
N(3)–Ru(1)–N(4)	177.5 (3)	Ru(2)–N(2)–C(6)	120.4 (7)
Ru(1)–Ru(2)–O(3)	92.6 (2)	Ru(1)–N(3)–C(11)	118.9 (7)
Ru(1)–Ru(2)–O(4)	92.0 (2)	Ru(1)–N(4)–C(16)	119.0 (5)
Ru(1)–Ru(2)–N(1)	88.9 (2)	O(1)–C(1)–N(1)	118.4 (8)
Ru(1)–Ru(2)–N(2)	88.3 (2)	O(2)–C(6)–N(2)	119.6 (9)
O(3)–Ru(2)–O(4)	175.4 (3)	O(3)–C11)–N(3)	119.9 (8)
O(3)–Ru(2)–N(1)	88.3 (3)	O(4)–C(16)–N(4)	118.8 (8)

[a] Numbers in parentheses are estimated standard deviations in the least significant digits.

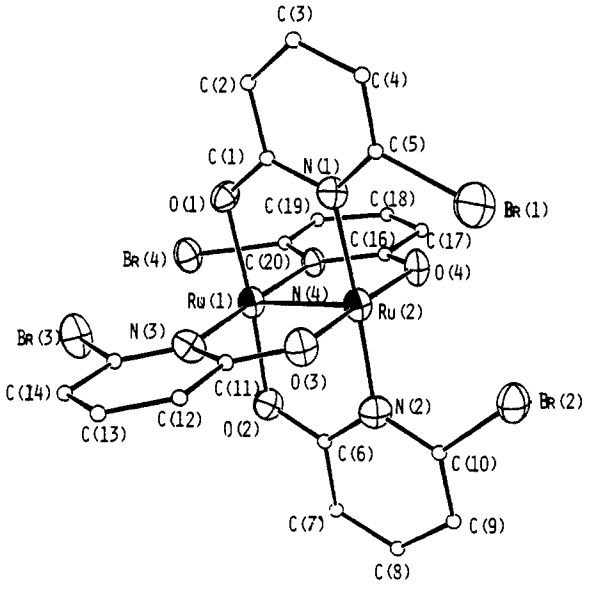

Figure 2. ORTEP drawing of $Ru_2(bhp)_4$.

Table IV. Selected Bond Distances (Å) and Angles (deg) for $[Ru_2(chp)_4]_2 \cdot CH_2Cl_2$

Bond Distances

atom 1–atom 2	distance[a]	atom 1–atom 2	distance[a]
Ru(1)–Ru(2)	2.247 (1)	Ru(4)–N(6)	2.103 (4)
Ru(1)–O(4)	2.040 (4)	Ru(4)–N(7)	2.094 (4)
Ru(1)–N(1)	2.074 (4)	O(1)–C(5)	1.294 (6)
Ru(1)–N(2)	2.110 (5)	O(2)–C(10)	1.295 (7)
Ru(1)–N(3)	2.078 (3)	O(3)–C(15)	1.304 (6)
Ru(2)–O(1)	2.047 (3)	O(4)–C(20)	1.302 (8)
Ru(2)–O(2)	2.041 (4)	O(5)–C(25)	1.292 (6)
Ru(2)–O(3)	2.072 (3)	O(6)–C(30)	1.291 (5)
Ru(2)–O(7)	2.265 (3)	O(7)–C(35)	1.321 (7)
Ru(2)–N(4)	2.112 (5)	O(8)–C(40)	1.265 (7)
Ru(3)–Ru(4)	2.247 (1)	N(1)–C(5)	1.357 (8)
Ru(3)–O(3)	2.290 (3)	N(2)–C(10)	1.362 (8)
Ru(3)–O(5)	2.045 (3)	N(3)–C(15)	1.356 (6)
Ru(3)–O(6)	2.056 (4)	N(4)–C(20)	1.373 (8)
Ru(3)–O(7)	2.077 (3)	N(5)–C(25)	1.368 (8)
Ru(3)–N(8)	2.106 (4)	N(6)–C(30)	1.361 (7)
Ru(4)–O(8)	2.049 (4)	N(7)–C(35)	1.343 (6)
Ru(4)–N(5)	2.076 (4)	N(8)–C(40)	1.385 (7)

Bond Angles

atom 1–atom 2–atom 3	angle[a]	atom 1–atom 2–atom 3	angle[a]
Ru(2)–Ru(1)–O(4)	90.0 (1)	O(5)–Ru(3)–O(7)	179.3 (1)
Ru(2)–Ru(1)–N(1)	88.0 (1)	O(5)–Ru(3)–N(8)	90.7 (2)
Ru(2)–Ru(1)–N(2)	88.2 (1)	O(6)–Ru(3)–O(7)	91.3 (1)
Ru(2)–Ru(1)–N(3)	88.8 (1)	O(6)–Ru(3)–N(8)	176.2 (1)
O(4)–Ru(1)–N(1)	92.1 (2)	O(7)–Ru(3)–N(8)	89.8 (1)
O(4)–Ru(1)–N(2)	178.0 (2)	Ru(3)–Ru(4)–O(8)	90.1 (1)
O(4)–Ru(1)–N(3)	84.3 (2)	Ru(3)–Ru(4)–N(5)	87.1 (1)
N(1)–Ru(1)–N(2)	89.0 (2)	Ru(3)–Ru(4)–N(6)	88.3 (1)
N(1)–Ru(1)–N(3)	175.1 (2)	Ru(3)–Ru(4)–N(7)	88.9 (1)
N(2)–Ru(1)–N(3)	94.6 (2)	O(8)–Ru(4)–N(5)	92.0 (2)
Ru(1)–Ru(2)–O(1)	89.7 (1)	O(8)–Ru(4)–N(6)	178.3 (2)
Ru(1)–Ru(2)–O(2)	89.3 (1)	O(8)–Ru(4)–N(7)	85.4 (2)
Ru(1)–Ru(2)–O(3)	90.2 (1)	N(5)–Ru(4)–N(6)	88.3 (2)
Ru(1)–Ru(2)–O(7)	161.81 (8)	N(5)–Ru(4)–N(7)	175.3 (2)
Ru(1)–Ru(2)–N(4)	87.6 (1)	N(6)–Ru(4)–N(7)	94.1 (2)
O(1)–Ru(2)–O(2)	89.7 (2)	Ru(2)–O(1)–C(5)	117.5 (4)
O(1)–Ru(2)–O(3)	178.5 (2)	Ru(2)–O(2)–C(10)	117.8 (3)
O(1)–Ru(2)–O(7)	106.1 (1)	Ru(2)–O(3)–Ru(3)	105.7 (2)
O(1)–Ru(2)–N(4)	90.1 (2)	Ru(2)–O(3)–C(15)	119.4 (3)
O(2)–Ru(2)–O(3)	88.8 (1)	Ru(3)–O(3)–C(15)	130.5 (2)
O(2)–Ru(2)–O(7)	82.0 (1)	Ru(1)–O(4)–C(20)	117.8 (4)
O(2)–Ru(2)–N(4)	176.8 (2)	Ru(3)–O(5)–C(25)	117.6 (3)
O(3)–Ru(2)–O(7)	73.8 (1)	Ru(3)–O(6)–C(30)	117.3 (3)
O(3)–Ru(2)–N(4)	91.5 (1)	Ru(2)–O(7)–Ru(3)	106.4 (2)
O(7)–Ru(2)–N(4)	101.1 (2)	Ru(2)–O(7)–C(35)	128.2 (3)
Ru(4)–Ru(3)–O(3)	160.86 (9)	Ru(3)–O(7)–C(35)	119.0 (3)
Ru(4)–Ru(3)–O(5)	90.5 (1)	Ru(4)–O(8)–C(40)	117.3 (3)
Ru(4)–Ru(3)–O(6)	89.3 (1)	Ru(1)–N(1)–C(5)	117.5 (3)
Ru(4)–Ru(3)–O(7)	89.2 (1)	Ru(1)–N(2)–C(10)	116.2 (4)
Ru(4)–Ru(3)–N(8)	87.1 (1)	Ru(1)–N(3)–C(15)	119.4 (3)
O(3)–Ru(3)–O(5)	107.2 (1)	Ru(2)–N(4)–C(20)	116.0 (4)
O(3)–Ru(3)–O(6)	84.0 (1)	Ru(4)–N(5)–C(25)	117.8 (3)
O(3)–Ru(3)–O(7)	73.1 (1)	Ru(4)–N(6)–C(30)	116.5 (3)
O(3)–Ru(3)–N(8)	99.8 (1)	Ru(4)–N(7)–C(35)	119.0 (4)
O(5)–Ru(3)–O(6)	88.1 (1)	Ru(3)–N(8)–C(40)	115.8 (3)

[a] Numbers in parentheses are estimated standard deviations in the least significant digits.

The ORTEP plots of the two independent $Ru_2(chp)_4$ units with the atom labels and the whole molecule are shown in Figures 3 and 4.

The most striking feature of this molecule is that the ligands take a polar arrangement around the metal centers so that one of the oxygen atoms on the $Ru_2(chp)_4$ can axially coordinate one of the Ru atoms on another such $Ru_2(chp)_4$ unit, and vice versa, to form a *dimer of the dimer*, i.e., $[Ru_2(chp)_4]_2$. Such a molecular geometry has been seen once before,[18] for $[Rh_2(mhp)_4]_2$. Because of the crowding of the chlorine atoms at each end of molecules, the polar arrangement imposes a large steric effect on the molecule. The average torsional angle is 20.4°, which is about the same as those previously reported for the polar compounds $Ru_2Cl(chp)_4$ and $Ru_2Cl(PhNpy)_4$.[19] The crowding of the molecule can also be seen from the ORTEP of the whole molecule. The structure is, however, quite stable, and this may be attributed to (1) the formation of $Ru-O_{ax}$ bonds and (2) the small rotation barrier about the Ru–Ru axis from the electronic configuration $\delta^{*2}\pi^{*2}$

(18) Berry, M.; Garner, C. D.; Hillier, I. H.; Clegg, W. *Inorg. Chim. Acta* **1980**, *45*, L209.

(19) Charkravarty, A. R.; Cotton, F. A.; Tocher, D. A. *Inorg. Chem.* **1985**, *24*, 1263.

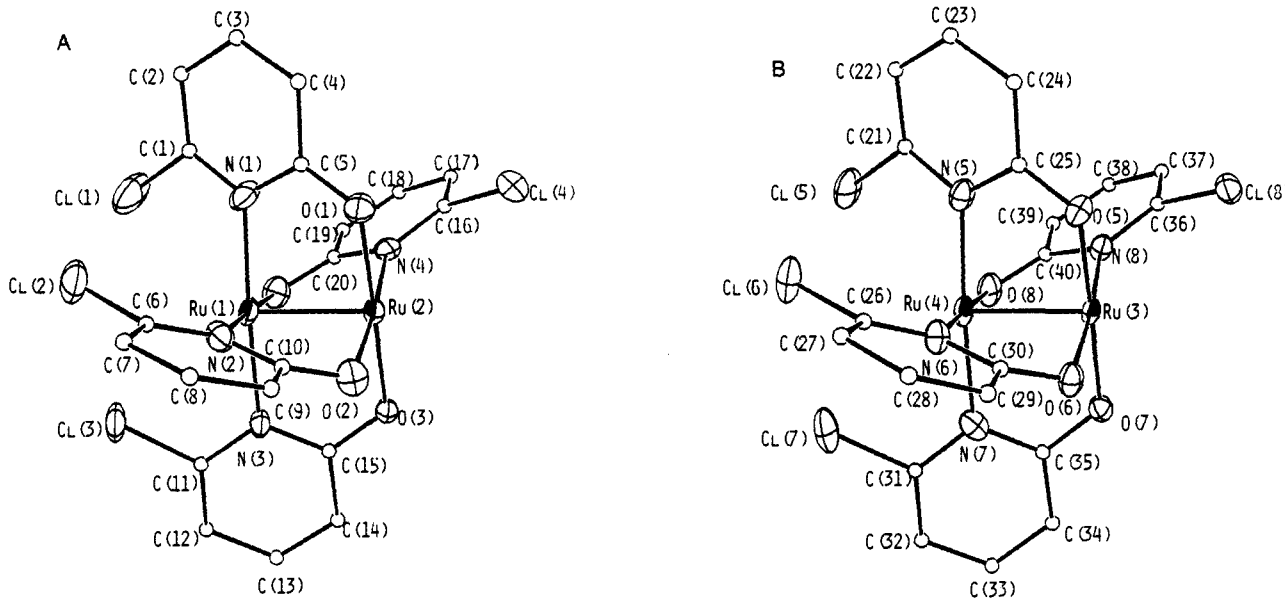

Figure 3. ORTEP drawings with the atom labels of the unit **1** and the unit **2** of $[Ru_2(chp)_4]_4$.

Table V. Selected Torsional Angles (deg)

$Ru_2(mhp)_4$	
atom 1–atom 2–atom 3–atom 4	angle[a]
N(1)–Ru(1)–Ru(2)–O(1)	−5.46 (0.15)
N(2)–Ru(1)–Ru(2)–O(2)	−6.14 (0.15)
O(3)–Ru(1)–Ru(2)–N(3)	−7.58 (0.14)
O(4)–Ru(1)–Ru(2)–N(4)	−5.74 (0.14)
$Ru_2(bhp)_4 \cdot 1.5C_6H_6$	
atom 1–atom 2–atom 3–atom 4	angle[a]
O(1)–Ru(1)–Ru(2)–N(1)	1.35 (0.25)
O(2)–Ru(1)–Ru(2)–N(2)	0.43 (0.26)
N(3)–Ru(1)–Ru(2)–O(3)	−1.37 (0.27)
N(4)–Ru(1)–Ru(2)–O(4)	−1.51 (0.27)
$[Ru_2(chp)_4]_2 \cdot CH_2Cl_2$	
atom 1–atom 2–atom 3–atom 4	angle[a]
N(1)–Ru(1)–Ru(2)–O(1)	20.55 (0.17)
N(2)–Ru(1)–Ru(2)–O(2)	21.21 (0.17)
N(3)–Ru(1)–Ru(2)–O(3)	15.37 (0.15)
O(4)–Ru(1)–Ru(2)–N(4)	22.59 (0.16)
O(3)–Ru(2)–O(7)–Ru(3)	7.91 (0.14)
O(5)–Ru(3)–Ru(4)–N(5)	21.29 (0.15)
O(6)Ru(3)–Ru(4)–N(6)	21.07 (0.16)
O(7)–Ru(3)–Ru(4)–N(7)	18.15 (0.15)
N(8)–Ru(3)–Ru(4)–O(8)	22.71 (0.16)

[a] Numbers in parentheses are estimated standard deviations.

(see discussion below). The Ru–Ru distance is 0.012 Å longer than that of $Ru_2(mhp)_4$ and 0.012 Å shorter than that of $Ru_2(bhp)_4$. Thus, there is no simple indication as to whether the Ru–Ru bond length is affected by the axial ligation. The geometry of the central M–O–M–O ring is generally determined by the overlap between the σ^*(M–M), which is collinear with the M–M axis, and the lone pair of the oxygen sp^2 hybrid. For $[Ru_2(chp)_4]_2$, the ring Ru(2)–O(3)–Ru(3)–O(7) is not planar; the torsional angle is 7.9°. The angles of Ru(1)–Ru(2)–O(7) and Ru(4)–Ru(3)–O(3) are 160.9° and 161.8°, respectively, which are smaller than the one in $[Rh_2(mhp)_4]_2$.[19] On the other hand, the Ru–O_{ax} distances are 2.265 Å for Ru(2)–O(7) and 2.290 Å for Ru(3)–O(3), and they are significantly longer than the one in the Rh analogue. The conclusion can be drawn that the M–O_{ax} interaction is stronger in the Rh case.

Magnetic Susceptibility Studies. The magnetic susceptibilities of all three compounds were measured from 5 to ca. 300 K. The molar magnetic susceptibilities χ_M were calculated from the measured χ_g and the molar diamagnetic corrections χ_D, which were also calculated on the basis of the Pascal constants.[20] From

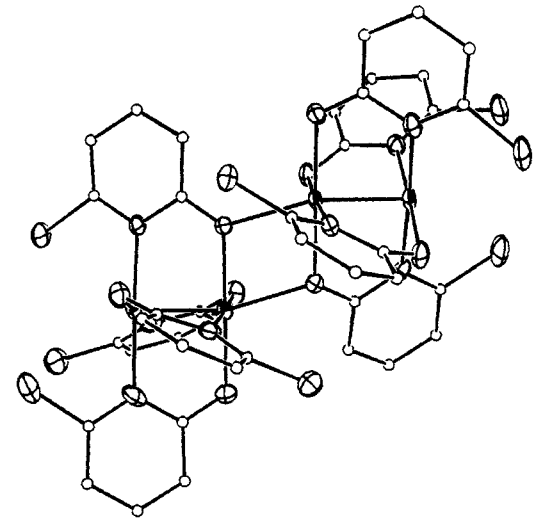

Figure 4. ORTEP drawing of the whole $[Ru_2(chp)_4]_2$.

Table VI. Parameters Related to the Magnetic Susceptibility[a]

parameter	$Ru_2(mhp)_4$	$Ru_2(bhp)_4$	$Ru_2(chp)_4$[b]
α	0.019	0.034	0.061
χ_D (cgs)	-297×10^{-6}	-360×10^{-6}	-318×10^{-6}
g_{eff}	1.55 (2)	1.77 (2)	1.86 (2)
D (cm^{-1})	208 (5)	248 (4)	232 (5)

[a] Numbers in parentheses following the values are esds occurring in the least significant digit. [b] Since the coupling between the two units of $Ru_2(chp)_4$ is weak (see text), the molecule is treated as two independent $Ru_2(chp)_4$.

the plots of χ_M vs T (Figures 5–7) it is easy to observe that there is always a rapidly rising tail when T approaches zero. This, as discussed before,[8] can be attributed to the presence of small amount of paramagnetic impurity. The impurity obeys the Curie law and is most likely $Ru_2(xhp)_4^+$. Similar to the case of $Ru_2(O_2CR)_4$, the χ_M can be expressed as

$$\chi_M = (1 - \alpha)\chi_0 + \alpha\chi_{imp} \quad (1)$$

Here α is the molar fraction of $Ru_2(xhp)_4^+$; χ_0 and χ_{imp} are the molar susceptibilities of $Ru_2(xhp)_4$ and $Ru_2(xhp)_4^+$, respectively.

(20) All the samples for the magnetic susceptibility measurement were crystallized from benzene and gently warmed (ca. 80 °C) under vacuum overnight. Hence, they were assumed to be solvent free.

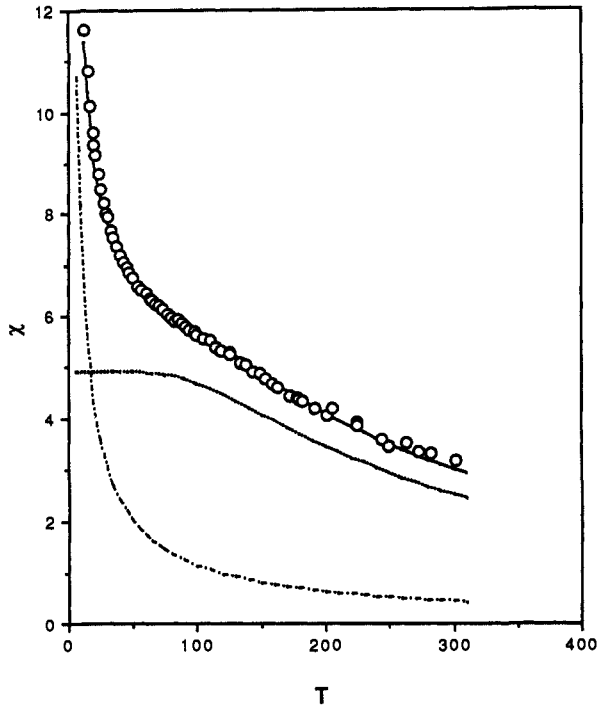

Figure 5. Magnetic susceptibility χ ($\times 10^3$ cgs) vs T (K) for $Ru_2(chp)_4$, where O gives the measured values, (-·-·-) the contribution of the impurity, (···) the contribution of $Ru_2(chp)_4$, and the solid line is calculated according to eq 2.

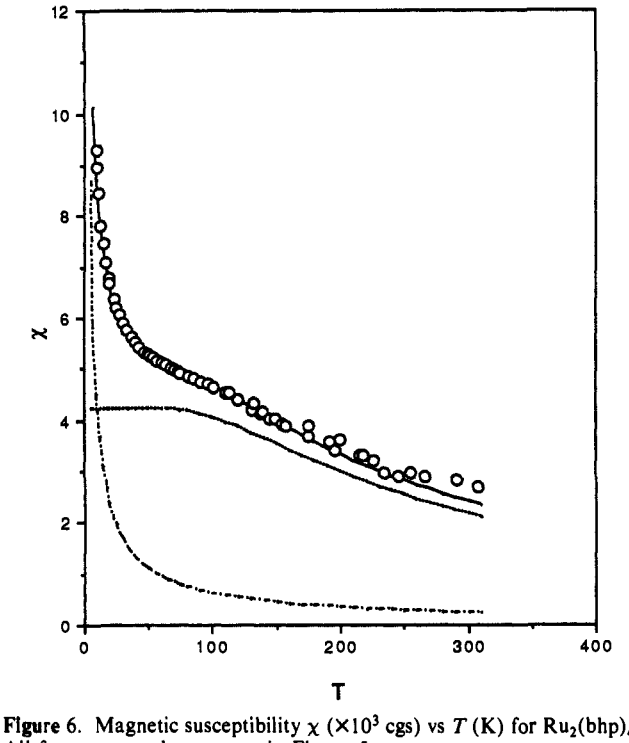

Figure 6. Magnetic susceptibility χ ($\times 10^3$ cgs) vs T (K) for $Ru_2(bhp)_4$. All features are the same as in Figure 5.

Since the magnetic susceptibility for $Ru_2(xhp)_4^+$ is not available at present, that of $Ru_2(but)_4C$[21] was used instead. This approximation would not affect our discussion at the qualitative level. The χ_0 is a constant in the low-temperature region ($T \leq 35$ K), and hence a linear least-squares fitting according to eq 1 gave the α value (see Table VI). The impurity content in the $Ru_2(mhp)_4$ sample was low, since it was treated with Na/Hg before recrystallization, while the contents were higher for both [$Ru_2(chp)_4$] and $Ru_2(bhp)_4$, due to the fact that they were recrystallized directly from the reaction products.

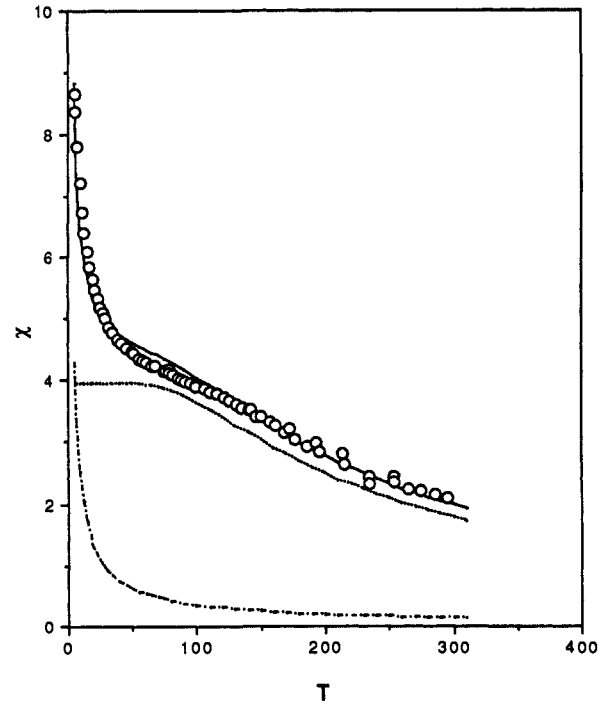

Figure 7. Magnetic susceptibility χ ($\times 10^3$ cgs) vs T (K) for $Ru_2(mhp)_4$. All features are the same as in Figure 5.

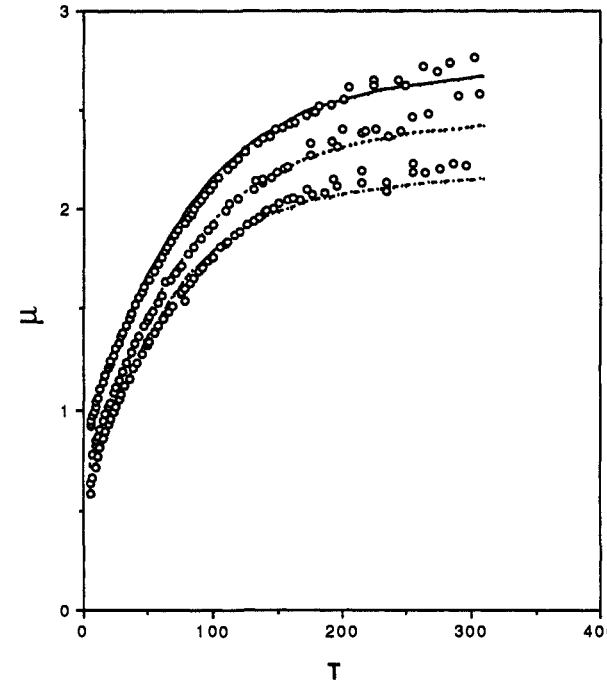

Figure 8. Magnetic moments μ (μ_B) vs T (K). Calculated values are as follows: $Ru_2(chp)_4$, (—); $Ru_2(bhp)_4$, (---); $Ru_2(mhp)_4$, (-·-·-); and (O) give all experimental values.

Generally, for the $Ru_2(LL)_4$[22] type compound with electronic configuration $\pi^{*2}\delta^{*2}$, the lowest energy state is $^3\Gamma$, where Γ is a one-dimensional representation of molecular symmetry group. Under the perturbation of the spin–orbit coupling, the $^3\Gamma$ will be split into a singlet ($M_S = 0$) and a doublet ($M_S = \pm 1$) with a separation D, which is usually called the zero-field splitting (ZFS).

(21) Telser, J.; Drago, R. S. *Inorg. Chem.* **1984**, *23*, 3114.

(22) LL is an abbreviation for any three-atom, uninegative, bridging bidentate ligand.

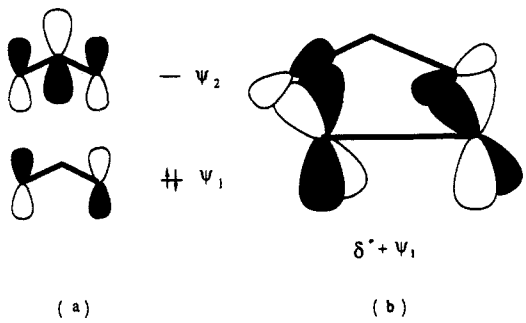

Figure 9. (a) Frontier orbitals of LL^-. (b) Overlap between the ψ_1 of LL^- and the δ^*(Ru–Ru).

The molar susceptibility for such a system, assuming that the singlet lies lowest, is

$$\chi = \frac{2Ng_{eff}^2\mu_B^2}{3k_BT} \frac{e^{-x} + \frac{2}{x}(1 - e^{-x})}{1 + 2e^{-x}} \quad (2)$$

Here $x = D/k_BT$, g_{eff} is the effective gyromagnetic ratio, k_B is Boltzmann constant, μ_B is the Bohr magneton, N is Avogadro's number, and T is the temperature (K).

To see if the electronic configuration of the $Ru_2(xhp)_4$ is $\pi^{*2}\delta^{*2}$, it is necessary to see if the susceptibility data can be fitted to eq 2. By a nonlinear least-squares fitting to eq 2, both D and g_{eff} were calculated for all three compounds and are listed in Table VI. The measured χ along with the simulated one (based on eq 2) for $Ru_2(mhp)_4$, $Ru_2(bhp)_4$, and $[Ru_2(chp)_4]_2$ are plotted in Figures 5–7. Also both experimental and simulated μ_{eff} (calculated according to $\mu_{eff}^2 = 3k_BT\chi/N$) for all three are plotted in Figure 8. From the fitting curve and the estimated standard deviations of the fitting parameters, it is obvious that the paramagnetism of the $Ru_2(xhp)_4$ complexes fits the model very well.[23] Besides, even from the experimental measured μ_{eff} curve (no any correction was included), a trend of μ_{eff} decreasing as T decreases can be easily observed, which also indicates the existence of a nonmagnetic ground state.

Discussion

Our results as well as the previous study[3] show that, for $Ru_2(xhp)_4$ complexes, the Ru–Ru bond lengths are in the range of 2.235 (1)–2.259 (1) Å, which are all shorter than the Ru–Ru distances in the known $Ru_2(xhp)_4^+$ species.[21,24,25] This, by the argument similar to that for the diruthenium carboxylate, favors the electron configuration $\delta^{*2}\pi^{*2}$. The magnetic susceptibility data give further strong support to this conclusion.

Generally for LL type ligands, the frontier orbitals are 3c–4e π orbitals, which are shown in Figure 9a. Among them, the ψ_1 is strictly symmetry adapted to the δ^* orbital of the diruthenium core (Figure 9b),[26] so an effective interaction that represents the π donation from LL^- to Ru–Ru core (we can call it the π basicity of LL^-) is expected. The stronger the π basicity of the LL^- ligand, the higher the δ^* orbital of $Ru_2(LL)_4$. The π basicity depends on the shape and the energy of ψ_1, which, in turn, are determined by the electronegativity of the atoms coordinated to the ruthenium atoms. In the RCO_2^- ligands, ψ_1 is relatively contracted and lies far below the δ^*. This gives a weak π basicity, which only pushes the δ^* closer to or about same as the π^* energy. In the $RNNNR^-$ ligand, on the other hand, ψ_1 is relatively expanded and lies closer to δ^*, because of the smaller electronegativity of nitrogen. Hence, it is a strong π base and can push the δ^* up so high that the δ^* is lies about 1 eV above π^*.[16] For the xhp^- ligands, a Fenske–Hall calculation[27] shows that in ψ_1 more than 65% of the π electron density is localized on the oxygen atom while less than 10% is on the nitrogen atom. Therefore, it is quite reasonable to see that the $Ru_2(xhp)_4$ compounds behave like the $Ru_2(O_2CR)_4$.

Acknowledgment. We thank the National Science Foundation for support of this work. We thank Professor J. L. Dye of Michigan State University for making his equipment available for the measurement of the susceptibility data and Dr. J. L. Colon of this department for assistance with the nonlinear least-squares calculation.

Supplementary Material Available: Complete tables of crystal data, positional parameters, bond distances and angles, anisotropic displacement parameters, and magnetic susceptibility data for **1–3** (43 pages); observed and calculated structure factors for the crystal structures of **1–3** (71 pages). Ordering information is given on any current masthead page.

(23) Due to the existence of the $Ru–O_{ax}$ bond, we would expect some interunit exchange interaction in the $[Ru_2(chp)_4]_2$ case. Since the fitting was good enough in the qualitative sense, the exchange constant J must be much smaller than D and hence can be ignored at the present stage.

(24) Charkravarty, A. R.; Cotton, F. A.; Tocher, D. A. *Inorg. Chem.* **1985**, *24*, 172.

(25) Charkravarty, A. R.; Cotton, F. A.; Schwotzer, W. *Polyhedron* **1986**, *5*, 1821.

(26) A simple drawing of the ψ_2 and π^* shows that they are essentially orthogonal, and therefore no other interactions exist.

(27) Cotton, F. A.; Ren, T. Unpublished result.